^{69,71}Ga NMR in the *kagomé* lattice compound $SrCr_{9-x}Ga_{3+x}O_{19}$

A. Keren* and P. Mendels
Laboratoire de Physique des Solides, URA2 CNRS, Université Paris Sud, 91405 Orsay, France

M. Horvatić
High Magnetic Field Laboratory, CNRS and Max-Planck-Institut für Festkörperforschung, Boîte Postal 166, 38042 Grenoble Cedex 9, France

F. Ferrer
Laboratoire de Physique des Solides, URA2 CNRS, Université Paris Sud, 91405 Orsay, France

Y. J. Uemura
Department of Physics, Columbia University, New York, New York 10027

M. Mekata and T. Asano
Department of Applied Physics, Fukui University, Fukui 910, Japan
(Received 29 May 1997)

We report the NMR site assignment of ^{69,71}Ga in the *kagomé* lattice compound $SrCr_{9-x}Ga_{3+x}O_{19}$, and discuss the couplings of the different Ga nuclei with Cr moments. We find that Ga($4e$) is dominantly coupled to the triangular plane, and Ga($4f$) is coupled to both the *kagomé* and triangular planes. The low-temperature behavior of the NMR signal in $SrCr_8Ga_4O_{19}$ suggests that a slowing down of some spin degrees of freedom occurs first on the *kagomé* plane. [S0163-1829(98)03717-5]

Recently the compound $SrCr_{9-x}Ga_{3+x}O_{19}$ [SCGO(x)] has been receiving considerable attention as a model system for antiferromagnetic spins on the *kagomé* lattice.[1–3] However, its crystal structure is not pure *kagomé* since it has Cr^{3+} ions (of spin 3/2) occupying both *kagomé* [Cr($12k$)] and triangular [Cr($2a$),Cr($4f$)] layers,[4,5] as shown in Fig. 1. Moreover, some Ga ions occupy the Cr($4f$) and Cr($12k$) layers for $x>0$ ($x=0$ is not stable).[4] Nevertheless, SCGO is considered to be a good example of a *kagomé* system because (i) the nonmagnetic Ga impurities are expected not to impact considerably the physical properties of the *kagomé* net,[6] (ii) the system shows two-dimensional character as demonstrated by neutron scattering,[5] and (iii) the superexchange coupling on the triangular lattice is expected to be much weaker than on the *kagomé* lattice (the ratio of the Cr-O length is ~ 2 between the two layers). In fact, the presence of two types of layers could be useful if one could probe them separately and compare their physical properties. As we show here, this can be done with ^{69}Ga and ^{71}Ga ($I=3/2$) NMR and NQR since there are two main types of Ga nuclei in the system: Ga($4e$) which is very close to the triangular planes and Ga($4f$) which is in between *kagomé* and triangular planes (see Fig. 1). The main purpose of the present work is to assign each site and nuclear spin transition to the corresponding peak in the NMR spectrum, although, in passing, we will also mention the magnetic properties of SCGO. In our next publication, these properties will be discussed extensively.[7]

The relevant part of the crystal structure is shown in Fig. 1. In the full structure the layers are stacked as follows: Cr($4f$)-Cr($12k$)-Cr($2a$)-Cr($12k$)-Cr($4f$)-Cr($4f$)-Cr($12k$), etc. The Ga($4f$) is in the center of a nearly ideal oxygen regular tetrahedron with Ga($4f$)-O distance of 1.864(6) Å. The broken lines in the figure represent such a tetrahedron. Since a regular tetrahedron has a local cubic symmetry, there cannot be an electric field gradient (EFG) in its center (and no quadrupole splitting). In contrast, one Ga($4e$)-O bond is different from the other three. This site belongs to the point symmetry D_{3h} and, in principal, will experience an EFG.

Our echo NMR experiments are performed on SCGO(x) at a constant applied frequency f_{app} and a varying external

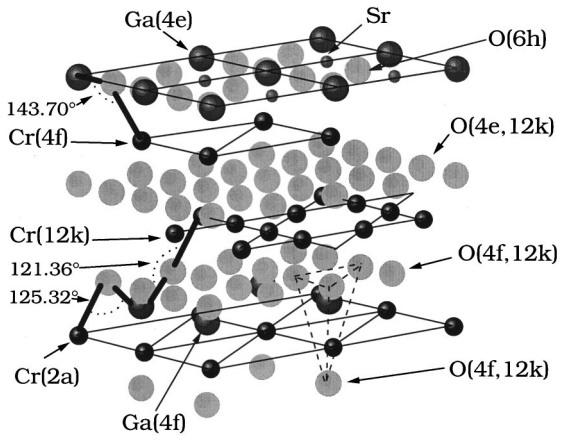

FIG. 1. The crystal structure of $SrCr_9Ga_3O_{19}$. The Cr($12k$) forms a *kagomé* lattice, and the Cr($4f$) and Cr($2a$) form a triangular lattice. The Ga($4f$) is in the center of an oxygen tetrahedron (with a local cubic symmetry), as shown by the broken line. The thick solid lines show possible hyperfine paths connecting a Ga to a Cr (see text).

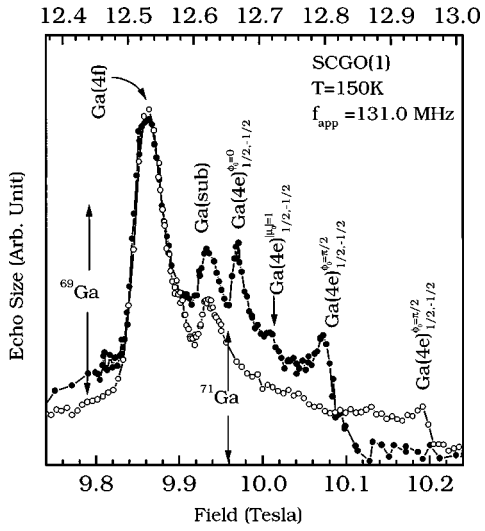

FIG. 2. A field sweep of ^{71}Ga and ^{69}Ga. The top abscissa is a rescale of the bottom one by a factor $^{71}\gamma/^{69}\gamma=1.27$. The closed (open) symbols represent ^{71}Ga (^{69}Ga). The site and transition assignment of each peak are described in the text. The Ga(sub) line is assigned to the Ga that substitutes Cr($4f$) sites. The $^{69}\mathrm{Ga}(4e)^{\varphi_0=0}_{1/2,-1/2}$ is hiding under the ^{69}Ga($4f$) peak.

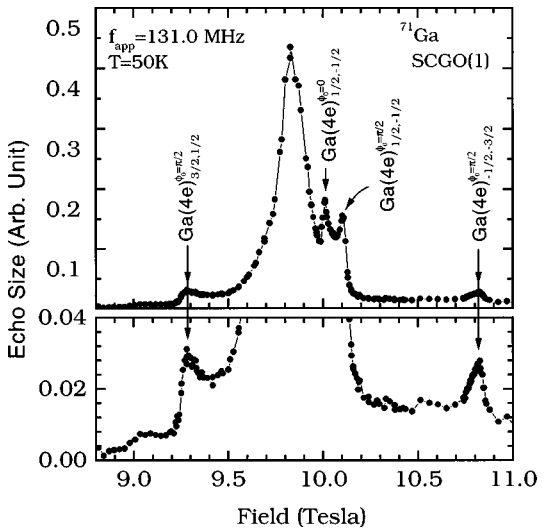

FIG. 3. A field sweep of ^{71}Ga. The bottom panel emphasizes the detection of satellite transitions.

magnetic field H_l. The echo amplitude is proportional to the number of spins for which f_{app} and H_l obey a resonance condition. For Ga nuclei which do not experience an EFG, e.g., Ga($4f$), all the nuclear transitions ($m\rightarrow m-1$) obey the resonance condition $f_{\mathrm{app}}\propto\gamma H_l$, where γ is the nuclear gyromagnetic ratio. On the other hand, in a powder sample, each transition of Ga nuclei which do sense an EFG, e.g., Ga($4e$), yields a resonance in a wide range of fields, with multiple peaks and steps appearing in the spectrum. The $3/2\leftrightarrow 1/2$ and the $-1/2\leftrightarrow -3/2$ transitions give rise to so-called satellite singularities, and the $1/2\leftrightarrow -1/2$ transition splits into two singularities also known as central line singularities.

In Fig. 2 we show two field sweeps of SCGO(1), obtained at $T=150$ K and $f_{\mathrm{app}}=131.0$ MHz: one between 9.74 and 10.3 T (bottom abscissa) covering the ^{71}Ga line ($^{71}\gamma/2\pi=12.982$ MHz/T, $^{71}Q=0.112\times10^{-24}$ cm^2), and the other between 12.37 and 13.08 (top abscissa) covering the ^{69}Ga line ($^{69}\gamma/2\pi=10.218$ MHz/T, $^{69}Q=0.178\times10^{-24}$ cm^2). The upper scale is linked to the bottom one by a factor $^{71}\gamma/^{69}\gamma=1.270$ so that all peaks that overlap correspond to Ga nuclei in a site without quadrupolar effects, therefore suggesting that the two peaks at $H_l=9.86$ and 9.93 T belong to a Ga in a cubic environment. On the other hand, the peaks of ^{71}Ga at $H_l=9.97$ and 10.07 T must be the two central line singularities of a Ga in a noncubic environment. We label them $^{71}\mathrm{Ga}(4e)^{\varphi_0=0}_{1/2,-1/2}$ and $^{71}\mathrm{Ga}(4e)^{\varphi_0=\pi/2}_{1/2,-1/2}$, respectively, where the subscript stands for the nuclear transition and the superscript stands for the angle (φ_0) in the powder average where a singularity is expected (see below). This assignment is supported by Fig. 3, where we depict a field sweep of ^{71}Ga at a temperature of 50 K and $f_{\mathrm{app}}=131.0$ MHz. In these favorable experimental conditions it is possible to detect the Ga($4e$) satellites singularities as emphasized in the lower panel. We label these two singularities $^{71}\mathrm{Ga}(4e)^{\varphi_0=\pi/2}_{3/2,1/2}$ and $^{71}\mathrm{Ga}(4e)^{\varphi_0=\pi/2}_{-1/2,-3/2}$. Another feature observed in the lower panel of Fig. 3 is a shoulder at 9 T. The origin of this shoulder is not clear to us at present.

The presence of satellites also implies that ^{71}Ga($4e$) has an NQR resonance frequency of $\sim$20 MHz and that ^{69}Ga($4e$) has an NQR resonance frequency 1.589 ($=^{69}Q/^{71}Q$) larger. Indeed, both resonances are found. In Fig. 4 we display a point by point frequency sweep ($H_l=0$) at a temperature of 80 K. Here, again, the top and bottom abscissa represent ^{69}Ga and ^{71}Ga, respectively, and are linked by the Q ratios. The fact that the lines of the two isotopes overlap implies that they are determined solely by the quadrupole interaction. The observation of the ^{69}Ga NQR frequency also suggests that the peak at $H_l=10.2$ T in Fig. 2 belongs to the upper field singularity of the ^{69}Ga central line. It is therefore labeled $^{69}\mathrm{Ga}(4e)^{\varphi_0=\pi/2}_{1/2,-1/2}$. The lower field singularity which we label $^{69}\mathrm{Ga}(4e)^{\varphi_0=0}_{1/2,-1/2}$ is hiding below the peak at 12.52 T [Ga($4f$) see below].

To distinguish between the peaks at $H_l=9.86$ and 9.93 T in Fig. 2, we compare in Fig. 5 a ^{69}Ga field sweep at T

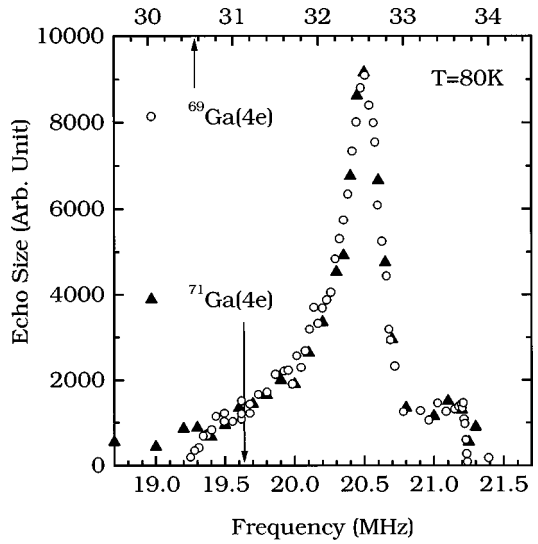

FIG. 4. A point by point frequency sweep at $H_l=0$ (NQR). The top abscissa is a rescale of the bottom one by a factor $^{69}Q/^{71}Q=1.589$.

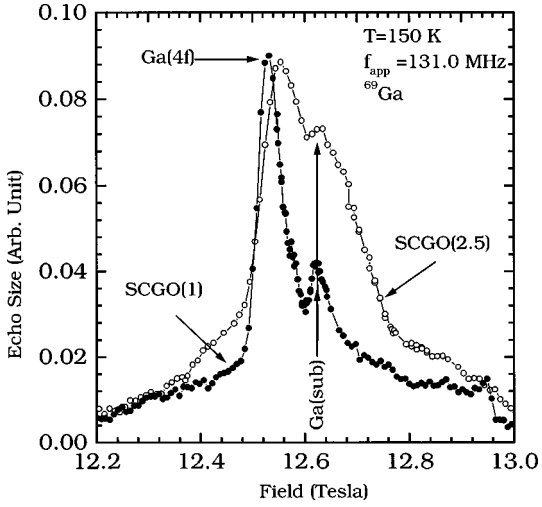

FIG. 5. A field sweep of ^{69}Ga in SCGO(x) for different values of x.

$=150$ K and $f_{\rm app}=131.0$ MHz in SCGO(1) with SCGO(2.5). Two elements are different between the samples, (i) the peak at $H_l=12.61$ T grows in intensity with respect to the peak at $H_l=12.52$ T when more Ga atoms are introduced and (ii) the shoulder at ~ 12.4 T grows in intensity for increasing x. We speculate that the $H_l=12.61$ T peak, and some underlying intensity which contributes to the shoulder, represent all nonstoichiometric gallium. We therefore label the ^{69}Ga peak at $H_l=12.61$ T (or ^{71}Ga at $H_l=9.93$ T) in Fig. 2 as Ga(sub), and at $H_l=12.52$ T (or ^{71}Ga at $H_l=9.86$ T) as Ga($4f$). The fact that the Ga(sub) peak position is proportional to γ suggests that it originates from a Ga atom substituting for Cr in a cubic environment. Therefore, the best candidate (although not perfect) for this peak is Ga in the Cr($4f$) site. From Fig. 2 it is also clear that the ratio of the linewidths of the ^{69}Ga($4f$) and ^{71}Ga($4f$) scale with the ratio of their γ. Therefore, the linewidth of the Ga($4f$) is determined by a distribution of either local fields or hyperfine couplings. Finally, it should be noted that it is no longer possible to distinguish between Ga($4f$) and Ga(sub) below $T=50$ K (see Fig. 3).

We now turn to discuss the possible couplings of Ga($4f$). The shift of the Ga($4f$) line at $T=50$ K is 0.025(7). This gallium could not be coupled to its neighboring Cr ions via dipolar interaction, since the expected dipolar shift is ~ 0.001. Therefore, we must consider the hyperfine option as dominant. There are three possible paths for this coupling, (i) Ga($4f$)-Cr($2a$), (ii) Ga($4f$)-O($4f$,12k)-Cr($2a$), (iii) Ga($4f$)-O($4f$,12k)-Cr(12k). Since Ga^{3+} and Cr^{3+} have filled $3d$ shells, hybridization between the two requires roughly 10 eV, and is very unlikely. On the other hand, the large and negative oxygen ion in the last two bonds (shown in Fig. 1 by a thick solid line) could create a covalent bridge connecting the Cr electronic spin with the Ga nucleus.[9] The Ga($4f$)-O($4f$,12k)-Cr($2a$) bond lengths are $R_{\rm Cr-O}=1.98$ Å, $R_{\rm Ga-O}=1.86$ Å, and the bond angle is $\theta=125.32°$; for the Ga($4f$)-O($4f$,12k)-Cr(12k) bond these parameters are $R_{\rm Cr-O}=2.06$ Å, $R_{\rm Ga-O}=1.86$ Å, and $\theta=121.36°$. The small difference in the angle and length between these bonds could lead to a stronger coupling to the Cr($2a$), however, the Ga($4f$) is coupled to 6 Cr(12k) and only 3 Cr($2a$), and we expect both planes to impact the Ga($4f$) roughly equally.

Next we discuss the nuclear Hamiltonian of Ga($4e$). In the spectrum of the Ga($4e$) at $T=50$ K (Fig. 3) there are four important field values: two for the central line singularities, and two for the satellites singularities. These values, together with the NQR frequency, constitute a set of five known numbers. If we assume that the principal axes of the shift tensor and that of the electric field gradient (EFG) are colinear then the nuclear spin Hamiltonian contains the same number of unknowns. We are therefore in a position to determine all Hamiltonian parameters from our powder spectrum. To do so, we write the Hamiltonian in the usual notation as

$$\mathcal{H}=-h\nu_l\mathbf{I}\cdot(\overline{\mathbf{1}}+\overline{\mathbf{K}})\cdot\hat{\mathbf{H}}_l+\frac{h\nu_q}{6}[3I_z^2-I^2+\eta(I_x^2-I_y^2)], \tag{1}$$

where $\nu_l=(\gamma/2\pi)H_l$, $\hat{\mathbf{H}}_l$ is a unit vector in the direction of the applied field, the principal axes of the shift tensor $\overline{\mathbf{K}}$ are colinear with the direction of the nuclear spin operators I_x, I_y, and I_z, ν_q is the NQR frequency (for $\eta=0$), and $0\leqslant\eta\leqslant 1$. In fact, we expect $\eta=0$ due to the threefold rotation symmetry of the Ga($4e$) site. The signal intensity for a given $m\leftrightarrow m-1$ nuclear spin transition P_m, is given by

$$P_m(H_l)\propto\int\delta[f_{\rm app}-\nu_m(H_l,\mu,\varphi)]d\Omega,$$

where the polar angles $\mu=\cos(\theta)$ and φ represent the orientation of the field with respect to the principal axes of the EFG tensor, and ν_m is the resonance frequency between the m and $m-1$ energy levels of the Hamiltonian. The full expression for $\nu_m(H_l,\mu,\varphi)$, which is usually obtained by a second order perturbation theory, is too long to be presented here and we refer the reader to Ref. 10.

A singularity in the spectrum will occur at a field which satisfies the equation

$$f_{\rm app}=\nu_m(H_l,\mu_0,\varphi_0) \tag{2}$$

for one of the values of m. The angles $\mu_0=\cos(\theta_0)$ and φ_0 are determined by two conditions:[11] (i) they are simultaneous solutions of the equations

$$\frac{\partial\nu_m}{\partial\mu}=0\quad\text{and}\quad\frac{\partial\nu_m}{\partial\varphi}=0, \tag{3}$$

and (ii) they correspond to a saddle point in the $\nu_m(H_l,\mu,\varphi)$ surface, namely,

$$D\equiv\left(\left[\frac{\partial^2\nu_m}{\partial\mu\partial\varphi}\right]^2-\left[\frac{\partial^2\nu_m}{\partial\mu^2}\right]\left[\frac{\partial^2\nu_m}{\partial\varphi^2}\right]\right)_{\mu=\mu_0,\varphi=\varphi_0}>0. \tag{4}$$

In Table I we present for each transition ($m\leftrightarrow m-1$) a (μ_0,φ_0) pair which solves Eqs. (3), and the resulting form of the resonance condition [Eq. (2)]. The shift values K_x, K_y, and K_z are assumed to be in the direction of the quadrupole principal axes. Also shown are the fields H_l in which the peaks were found experimentally. It should be pointed out that the values of the Ga($4e$) $1/2\leftrightarrow -1/2$ peak position do not change within experimental accuracy when the

TABLE I. The equations relating the applied frequency to external field at which a peak is found in a powder average of a spin 3/2 for relevant μ_0 and φ_0 (see text). H_l is the field where each peak was found experimentally at $T=50$ K (see Fig. 3).

Transition	$\mu_0=$	$\varphi_0=$	$f_{\rm app}=131.0$ MHz$=$	H_l (T)
$3/2\leftrightarrow 1/2$	0	$\pi/2$	$\frac{1}{2}\nu_q(1-\eta)+(1+K_x)\nu_l$	9.282
$1/2\leftrightarrow -1/2$	0	0	$\frac{\nu_q^2}{48\nu_l}(9-6\eta+\eta^2)+(1+K_y)\nu_l$	10.012
$1/2\leftrightarrow -1/2$	$\sqrt{\frac{8\nu_l^2(K_x-K_z)+\nu_q^2(15-8\eta+\eta^2)}{3(3-\eta)^2\nu_q^2}}$	$\pi/2$	$-\frac{\nu_q^2}{3\nu_l}(1-\eta)-\frac{2K_x(\eta-2)+K_z(\eta-5)+3(\eta-3)}{3(3-\eta)}\nu_l$ $-\frac{4(K_x-K_z)^2\nu_l^3}{3\nu_q^2(\eta-3)^2}$	10.110
$-1/2\leftrightarrow -3/2$	0	$\pi/2$	$-\frac{1}{2}\nu_q(1-\eta)+(1+K_x)\nu_l$	10.827

Ga($4f$) peak is fitted to a Lorentzian and subtracted from the data. To these four equations we must add the NQR relations[12] (at $T=50$ K) $f_{\rm app}=20.65(30)$ MHz $=\nu_q\sqrt{1+\eta^2/3}$. This gives five equations with five unknowns. The only physical solution ($\nu_q>0$ and $0\leqslant\eta\leqslant 1$) of these equations which also obeys $D>0$ is $K_x=0.0035(10)$, $K_y=0.0035(10)$, $K_z=0.0085(10)$, $\nu_q=20.5(3)$, and $\eta=0.050(35)$. The errors are governed mostly by the width of the NQR line.

However, for each value of m there is more than one pair (μ_0,φ_0) which obeys Eqs. (3). When trying to find the Hamiltonian parameters for all other possible pairs we find that they do not produce physical solutions or do not obey $D>0$ as required in Eq. (4). Thus, under the colinearity assumption for the principal axes, the parameters given above are unique. Moreover, the small value found for η is in agreement with our expectation. We also perform a consistency test by calculating the position of the step expected from the $1/2\leftrightarrow -1/2$ transition at $|\mu_0|=1$ and $T=150$ K. We predict it to be at $H_1=9.99$ T. Experimentally this step is found at 10.00 T as shown in Fig. 2 and is therefore labeled $^{71}{\rm Ga}(4e)^{|\mu_0|=1}_{1/2,-1/2}$.

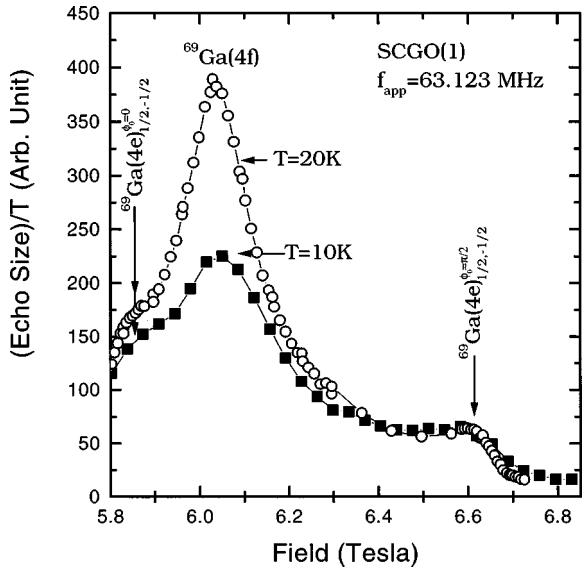

FIG. 6. A field sweep of ^{69}Ga at different temperatures.

Finally, our analysis shows that the Ga($4e$) has a smaller shift than that of Ga($4f$) but it is still strong enough to be governed by hyperfine coupling. In fact, even the anisotropy in the shift could not be explained by dipolar coupling. Since Ga($4e$) is very close to the triangular layers it must be coupled mostly to it via the Ga($4e$)-O($6h$)-Cr($4f$) path (shown in Fig. 1 by a thick solid line). The bond parameters are $R_{\rm Cr-O}=2.00$ Å, $R_{\rm Ga-O}=1.83$ Å, and $\theta=143.36$. These parameters are very close to those of the Ga($4f$)-O($4f$,12k)-Cr(12k) bond and the Ga($4e$) should have roughly the same coupling strength to a Cr on the triangular plane as Ga($4f$) to a Cr on the *kagomé* plane.

This result allows us to probe the spin dynamics in the *kagomé* and triangular planes separately, as we shall show thoroughly in a forthcoming paper. For example, we can follow the temperature dependence of the Ga($4f$) spectra. In Fig. 6 we depict field scans at $f_{\rm app}=63.125$ MHz and temperatures of 20 and 10 K. At this applied frequency, the ^{69}Ga($4f$) peak is in between the $^{69}{\rm Ga}(4e)^{\varphi_0=0}_{1/2,-1/2}$ (which was hiding in Fig. 2) and the $^{69}{\rm Ga}(4e)^{\varphi_0=\pi/2}_{1/2,-1/2}$ peaks. The intensity is calibrated so that the $^{69}{\rm Ga}^{\varphi_0=\pi/2}_{1/2,-1/2}$ satellite has the same intensity (corrected by temperature effects) for both lines. It is clear from this figure that as the temperature decreases, the ^{69}Ga($4f$) line broadens (and loses intensity[7]) much more than that of ^{69}Ga($4e$). This, in fact, is a well-known NMR phenomenon near a phase transition of the spin-glass type[8] and, indeed, in SCGO a spin-glass-like phase transition is observed at $T_f=3.5$ K (Ref. 2) by susceptibility measurements. Therefore, it seems that at temperatures where the Ga($4e$) is not yet experiencing slowing down of the spin fluctuations, the Ga($4f$) does. Thus any freezing occurs first on the *kagomé* plane. This example demonstrates that the different planes in SCGO can be probed separately with Ga NMR.

We would like to thank M. Eremin, H. Alloul, and C. Berthier for helpful discussion, and LCMI for the use of the high magnetic field facility and kind hospitality.

*Now at Technion-Israel Institute of Technology, Department of Physics, Haifa 32000, Israel.

[1] C. Broholm, G. Aeppli, G. P. Espinosa, and A. S. Cooper, Phys. Rev. Lett. **65**, 3173 (1990); A. P. Ramirez, G. P. Espinosa, and A. S. Cooper, Phys. Rev. B **45**, 2505 (1992); Y. J. Uemura *et al.*, Phys. Rev. Lett. **73**, 3306 (1994); P. Schiffer, A. P. Ramirez, K. N. Franklin, and S.-W. Cheong, *ibid.* **77**, 2085 (1996).

[2] A. P. Ramirez, G. P. Espinosa, and A. S. Cooper, Phys. Rev. Lett. **64**, 2070 (1990); B. Martinez *et al.*, Phys. Rev. B **46**, 10 786 (1992).

[3] B. Martínez, A. Labarta, R. Rodríguez Solá, and X. Obradors, Phys. Rev. B **50**, 15 779 (1994).

[4] X. Obradors, A. Labarta, A. Isalgué, J. Tejada, and J. R. M. Pernet, Solid State Commun. **5**, 189 (1988).

[5] S. H. Lee, C. Broholm, G. Aeppli, T. G. Perring, B. Hessen, and A. Taylor, Phys. Rev. Lett. **76**, 4424 (1996).

[6] E. F. Shender, V. B. Cherepanov, P. C. W. Holdsworth, and A. J. Berlinksy, Phys. Rev. Lett. **70**, 3812 (1993); A. Keren, J. Magn. Magn. Mater. **140-144**, 1493 (1995).

[7] P. Mendels *et al.* (unpublished).

[8] D. E. MacLaughlin and H. Alloul, Phys. Rev. Lett. **36**, 1158 (1976).

[9] M. V. Eremin and O. G. Khutsishvili, Sov. Phys. Solid State **29**, 1546 (1987).

[10] R. B. Creel, S. L. Segel, R. J. Schoenberger, R. G. Barnes, and D. R. Torgeson, J. Chem. Phys. **60**, 2310 (1974).

[11] J. F. Baugher, P. C. Taylor, T. Oja, and P. J. Bary, J. Chem. Phys. **50**, 4914 (1969).

[12] A. Abragam, *Principles of Nuclear Magnetism* (Oxford University Press, Oxford, 1989), Chap. VII.